

Influence of sawdust particle size on fired clay brick properties

G. Thalmaier^a✉, N. Cobîrzan^a, A.-A. Balog^a, H. Constantinescu^a, M. Streza^b,
M. Nasui^a, B.V. Neamtu^a

a. Technical University of Cluj Napoca, Cluj, Romania

b. National Institute for Research and Development of Isotopic and Molecular Technologies, Cluj-Napoca, Romania
✉ Gyorgy.Thalmaier@sim.utcluj.ro

Received 27 March 2019
Accepted 1 October 2019
Available on line 19 March 2020

ABSTRACT: This study investigates the effect of adding different size fractions of the same pore forming agent (sawdust) on the material's compressive strength and heat transfer. The samples were dry pressed and fired at high temperature inside an oven. Phase transformations were evidenced by a combination of differential thermal analysis, thermogravimetry and mass spectrometry (DTA-TGA-MS) and X-ray diffraction (XRD) techniques, in the temperature range of 24-900 °C. Image analysis (IA) and compression tests were performed to explain the mechanical behaviour of the samples. The thermal conductivity was obtained by using combined photopyroelectric calorimetry (PPE) and lock-in thermography (LIT) techniques. The pressing direction has an impact on the distribution of pores and the heat transfer by conduction.

KEYWORDS: Brick; Compressive strength; Thermal analysis; Wood; Pore size distribution.

Citation/Citar como: Thalmaier, G.; Cobîrzan, N.; Balog, A.-A.; Constantinescu, H.; Streza, M.; Nasui, M.; Neamtu, B.V. (2020) Influence of sawdust particle size on fired clay brick properties. *Mater. Construcc.* 70 [338], e215 <https://doi.org/10.3989/mc.2020.04219>

RESUMEN: *Influencia del tamaño de partícula del serrín en las propiedades de los ladrillos de arcilla quemada.* Este estudio investiga el efecto de la adición de diferentes fracciones de tamaño del mismo agente de formación de poros (serrín) sobre la resistencia a la compresión y la transferencia de calor del material. Las muestras fueron presionadas, secadas y cocidas a alta temperatura dentro de un horno. Se identificaron transformaciones de fase mediante el empleo de análisis térmico diferencial, termogravimétrico y espectrometría de masas (DTA-TGA-MS) y técnicas de difracción de rayos X (XRD) en el intervalo de temperatura de 24-900^oC. Se realizaron análisis de imagen (IA) y ensayos de compresión para explicar el comportamiento mecánico de las muestras. La conductividad térmica se obtuvo mediante el uso de técnicas combinadas de calorimetría fotopiroeléctrica (PPE) y termografía de bloqueo (LIT). Se concluye que la dirección de prensado tiene un impacto sobre la distribución de los poros y la transferencia de calor por conducción.

PALABRAS CLAVE: Ladrillo; Resistencia a la compresión; Análisis térmico; Madera; Distribución de tamaño de poro.

ORCID ID: G. Thalmaier (<https://orcid.org/0000-0003-2762-6110>); N. Cobîrzan (<https://orcid.org/0000-0002-6904-0436>); A.-A. Balog (<https://orcid.org/0000-0002-3587-6438>); H. Constantinescu (<https://orcid.org/0000-0003-3290-3290>); M. Streza (<https://orcid.org/0000-0002-0030-8625>); M. Năsui (<https://orcid.org/0000-0002-4792-2032>); B.V. Neamtu (<https://orcid.org/0000-0003-0666-8303>)

Copyright: © 2020 CSIC. This is an open-access article distributed under the terms of the Creative Commons Attribution 4.0 International (CC BY 4.0) License.

1. INTRODUCTION

Energy saving in buildings may be achieved by using materials with high thermal performance (1). The easiest way to improve the thermal performance of solid fired-clay bricks is to increase their porosity. It is well known that thermal conductivity and mechanical properties are strongly influenced by void fraction with a direct effect: an increase of the porosity increases thermal performance but decreases mechanical strength. This limits the maximum porosity to levels that ensures a reasonable mechanical strength, for specific application requirements in constructions (2-6). Principal factors which affect the materials values of thermal conductivity and mechanical strength are their microscopic and macroscopic structure (pore volume, size and shape), mineralogical composition and anisotropy (7-12).

For solid clay units the reduction of the thermal conductivity parameter may be obtained by incorporating different waste materials which play the role of pore-forming agents (6, 13-18). The well-known pore forming agents' materials incorporated up to now into clay matrix by scientific researchers are residual biomass (15, 18), paper waste (6, 16), vermiculite (19), etc.

An efficient pore forming agent is a building material with high content of organic matter, which has the role to improve the thermal properties of ceramic materials by increasing their porosity. One of the waste materials which can be used as an organic pore forming agent is sawdust. In the clay matrix it plays multiple roles: act as a pore forming agent which burns during the firing, increasing the porosity and reducing the thermal conductivity (12, 15) of the final product and save energy in the manufacturing process, due to its high caloric power (15-20, 5MJ/kg) (20).

Based on studies performed by other authors, sawdust content into the clay matrix is up to 30% (11, 15, 21-24), depending by the raw material characteristics.

Depending on the particle size, the sawdust in the firing process will develop in the clay matrix a network of different types of pores (capillary, subcapillary or microcapillary pores). In ceramic specimens these pores are supplementary to those resulted due to the clay's particle arrangement and those resulted during the chemical and mineralogical transformations which appear at different firing temperatures (12).

The study investigates the influence of sawdust particles size on mechanical and thermal properties of solid fired clay bricks, and the anisotropy of porosity and thermal conductivity measured in two directions (parallel and perpendicular to the pressing direction). The aim of the experimental study was to determine the influence of the pore size in improving the thermal properties of fired clay

bricks while the mechanical properties are kept in acceptable limits.

2. EXPERIMENTAL PROCEDURES

2.1. Sample preparation

The raw materials used for clay brick samples consists of clays (a mixture of yellow and grey clay, 30:70 ratio) and 15 vol.% sawdust sieved to different size fractions, as follows: <0.2mm; 0.315 - 0.4mm; 0.5 - 0.63mm; 0.63 - 0.8mm; 0.8 - 1.2mm. The used percentage of sawdust was determined from preliminary experiments as being the 15 vol. % in order to keep the values of mechanical properties above the admissible value. Approximately 10 vol. % water was added to increase the presability of the mixture. The mixture has a wide size distribution with particle size < 6 mm and $D_{50} \sim 2$ mm, as presented in Figure 1a. The yellow and gray clays particles size distribution was measured by light scattering on a Fritsch Analysette 22 laser particle size analyser (Figure 1b,c).

Beside the samples containing sawdust particles some control bricks were manufactured without pore forming agent. The samples were pressed at 20MPa in a hardened steel mould, the samples dimensions 15x15x15mm.

The heat cycle used for firing started with a slow heating rate (1.5 °/min) from room temperature to 90 °C and this temperature was maintained for 60 minutes for a thorough drying of the samples. The temperature was further increased at a rate of 5°/min up to 600°C then with 2°/min up to 900 °C where it was maintained for 2h. The cooling curve begins with a decrease (5 °/min) down to 670 °C, and then the cooling rate was decreased to 1.5°/min to avoid the cracking caused by the quartz phase transformation. After 570°C the samples were furnace cooled to room temperature.

The chemical and mineralogical analysis of samples were determined in a previous study (6).

2.2. Investigation methods

2.2.1. Method used

The phase transformations were evidenced in the 25-900 °C temperature range by a combination of X-ray diffraction (Equinox D3000 diffractometer with Co radiation) and DTA-TGA (10°/min - in air) thermal analysis combined with mass spectrometry.

The water absorption, bulk density and compressive strength were determined as the average values obtained on five cubic specimens 15x15x15mm.

First the samples were dried into an oven at 105°C \pm 5 °C until a constant mass, and then the water content of the specimens was expressed according to SR EN 772-21: 2011 (25), as ratio between the wet and dried mass of the samples.

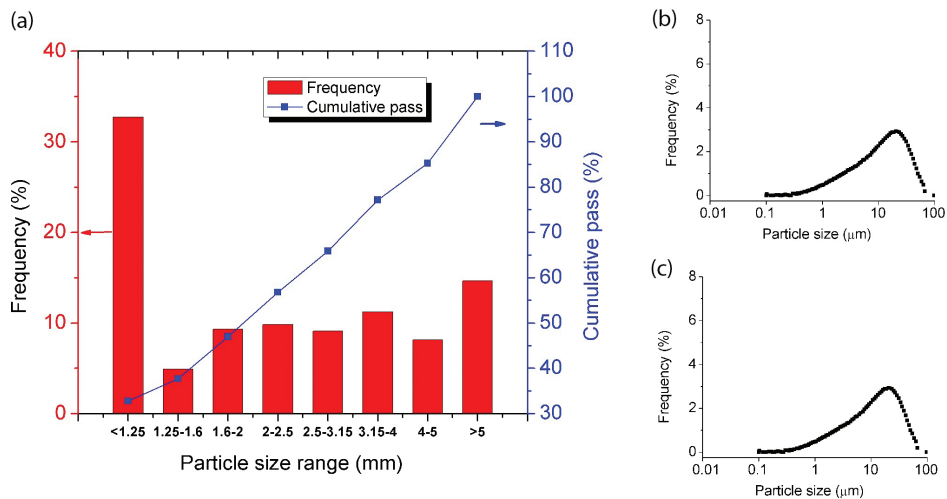


FIGURE 1. a) The press-ready mixture’s particle size distribution obtained by sieving, the yellow b) and gray c) clays particle size distribution.

The bulk density of samples was calculated based on SR EN 772–13:2001 (26) by measuring the samples dimensions and dividing the mass by the calculated volume. The material’s density was measured by pycnometry and used to determine the total porosity of the samples. The pore size distribution was measured by image analysis (on optical images using ImageJ software), the measured areas of the pores were transformed into equivalent diameters considering spherical pores with identical areas.

The total porosity was calculated $P = (1 - \text{Bulk density} / \text{Solid density}) \times 100$, where the solid density was measured in each case by pycnometry.

A Controls Advantest 9 hydraulic press with a load rate of 0.2 MPa/s, and the accuracy of the force recording of 0.01MPa, was used in order to determine the specimens’ compressive strengths.

The thermal effusivity of the samples was obtained by using the PPE technique in the front configuration (FPPE), while non-contact infrared lock-in thermography technique (LIT) was used to get their thermal diffusivity (27). Knowing the values of the thermal effusivity and thermal diffusivity, the thermal conductivity was calculated according to the following Equation [1]:

$$k = e (\alpha)^{1/2} \tag{1}$$

where α is the thermal diffusivity, e is the thermal effusivity and k is the thermal conductivity of the investigated sample.

2.2.2. Theoretical aspects

The temperature variation of a sample exposed to a modulated radiation can be measured with a pyroelectric sensor. In the front detection configuration (FPPE) the sensor is first irradiated, and the

investigated sample is placed directly on the pyroelectric sensor. For an optically opaque sensor, the radiation is absorbed on its front electrode and converted into heat. The developed heat propagates through both the sensor and the sample. Due to the thermal gradient between the two electrodes of the sensor, a complex electrical signal is generated. The amplitude and the phase of the signal depends on the thermal parameters of the sample. For a thermally thick sensor and sample, the phase of the PPE signal is given by Equations [2] and [3]:

$$\tan \Theta = \frac{(1 + R_{mp}) \exp(-x) \sin(x)}{1 - (1 + R_{mp}) \exp(-x) \cos(x)} \tag{2}$$

$$\text{with } x = a_p L_p \text{ and } \frac{e_m}{e_p} = \frac{1 + R_{mp}}{1 + R_{mp}} \tag{3}$$

R_{mp} represents the reflection coefficient of the thermal wave at the interface material (m)-sensor (p), L_p is the thickness of the sensor, and a_p is the reverse of the thermal diffusion length ($a_p = 1/\mu$). The thermal diffusion length is $\mu = (\alpha/\pi f)^{1/2}$ with f the modulation frequency.

The thermal effusivity of the sample can be measured by performing a frequency scan of the phase of the PPE signal, according to Equations [2] – [3].

The thermal diffusivity of solid samples by using the lock-in thermography technique can be calculated from the shift of the phase (which is a time delay in the propagation of the thermal wave as compared to a reference signal). The phase shift $\Delta\phi$ has the following expression [4]:

$$\Delta\phi = -\sqrt{\frac{\pi f}{\alpha}} x = ax \tag{4}$$

where x is the distance from the punctual heat source, $a = l/\mu$ is the slope of the phase versus distance plot and f is the excitation frequency. At a big distance from the punctual heat source, the thermal wave can be approximated by a plane wave and accordingly, the thermal diffusivity can thus be calculated according to Equation [4].

3. RESULTS AND DISCUSSIONS

The XRD pattern of the starting mixture (Figure 2) consists of quartz, kaolinite, calcite, dolomite and some iron oxides. Part of these phases suffer transformations during the firing process.

Part of the phase transformations that occur during the firing process are associated with heat effects, so these transformations are also monitored by thermal analysis. The DTA-TGA curve is presented in Figure 3. The water evaporation, the carbonates decomposition and the burning of the added biomass are the main cause of weight loss in brick manufacturing.

The first effect visible in the TGA curve is a wide endothermic peak corresponding to the water evaporation. This water evaporation starts at temperatures over 50 °C and is still ongoing up to temperatures around 200 °C. The second effect present is a strong exothermic peak composed of several effects. The major effect is the burning of the sawdust particles in the 270–620 °C temperature range. Over this range a smaller endothermic effect is overlapping, the kaolinite- metakaolinite transformation with the release of the OH functional group. Further increasing the temperature, the carbonates'

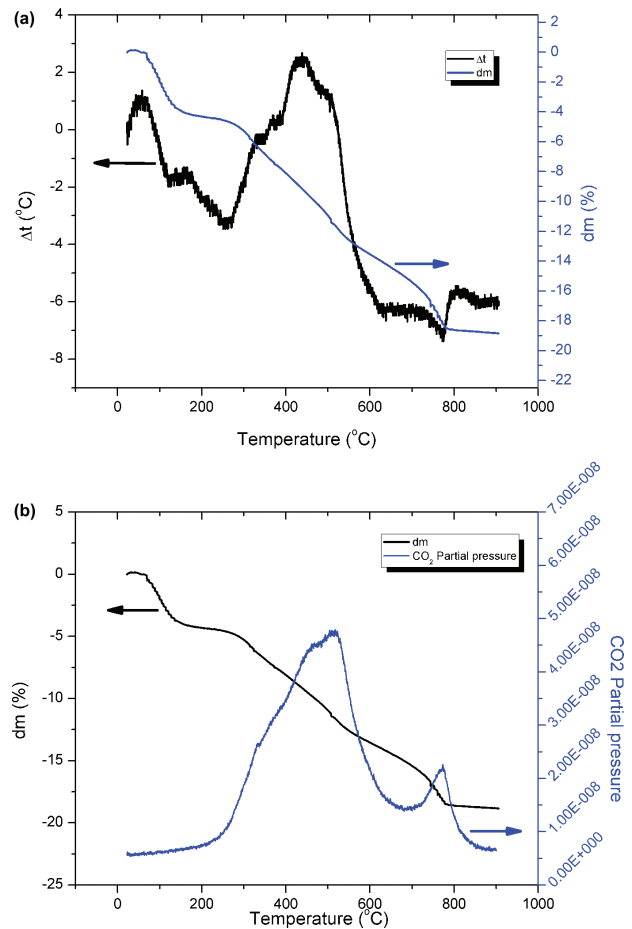


FIGURE 3. DTA-TGA-MS analysis of the starting mixture: a). DTA-TGA curve, b). CO₂ partial pressure variation.

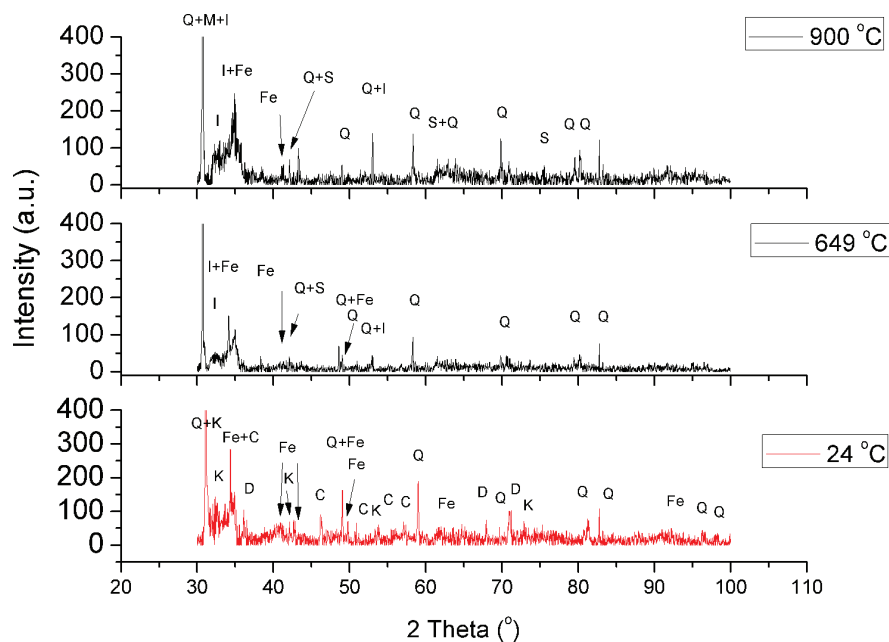


FIGURE 2. X ray diffraction (Q –quartz, K- Kaolinite, Fe- iron oxides, C- calcite, D- dolomite, I- illite, S –Iron silicon oxide).

decomposition begins. During firing, carbonates act as pore-forming agents and generate crystalline phases, which can enhance mechanical strength (28). The calcium carbonate that begins to decompose as the CO_2 partial pressure indicates, around 700°C and continues up to 860°C . These observations are similar with the findings of other authors on clays (29). No clear evidence of liquid forming was observed in the DTA-TGA analysis.

Samples contains no pore-forming agent except for the naturally occurring carbonates having densities of 1.69g/cm^3 (control sample-CS). By adding sawdust, the other samples had their density reduced by approximately 12-17% and are presented in Table 1. Some scattering of the results was observed but they remained within acceptable limits and were due to the uneven nature of the naturally occurring materials.

An increase of the total porosity by 11-13% was observed, some of the porosity was lost during the firing shrinkage.

TABLE 1. The obtained bulk density, water absorption and total porosity.

Sample	Sawdust size fraction [mm]	Bulk density [g/cm^3]	Water absorption [%]	Total porosity [%]
CS	-	1,69	18	25
M1	<0.2	1,45	23.7	36
M2	0.315 - 0.4	1,39	22.6	39
M3	0.5 - 0.63	1,40	24.4	38
M4	0.63 - 0.8	1,38	23.1	40
M5	0.8 - 1.2	1,38	24.5	37

The water absorption properties of bricks are a key factor that affects their durability and describes the open porosity through which water can pass. An important increase ($\sim 30\%$) in the water absorption was obtained by the addition of the sawdust and it is also visible in the total porosity increase. Most of the pores responsible for the water absorption are capillary pores which represent about 23% of the total volume. These pores are generated by two mechanisms: gas releases during the firing representing about 16% (5 % from water and 11 % from calcium carbonate) and 7% from the clay particle arrangement. The difference (up to total porosity) is given by the sawdust particles after burning.

The anisotropic nature of the sawdust particle gives another unusual effect in the samples; the orientation of the pore former in the die's filing direction. This effect was evidenced by measuring the porosity in the transversal and longitudinal direction by image analysis. The results are presented in Figure 4. Since the porosity is the main factor that affects the compressive strength and the thermal conductivity, it is important to take these variations into account.

In the fired bricks, the carbonates from the raw materials and the interparticle voids are responsible for generating micrometer sized pores. The large pores generated by the burning of the organic particles create a pore network that can compromise the brick's properties by acting as a weak link. These large pores (millimetre sized), are easily visible by optical microscopy. Using the ImageJ software, the pore size distribution of the different samples was measured on transversal and longitudinal direction for five samples for each sample type. The results are presented in Figure 5.

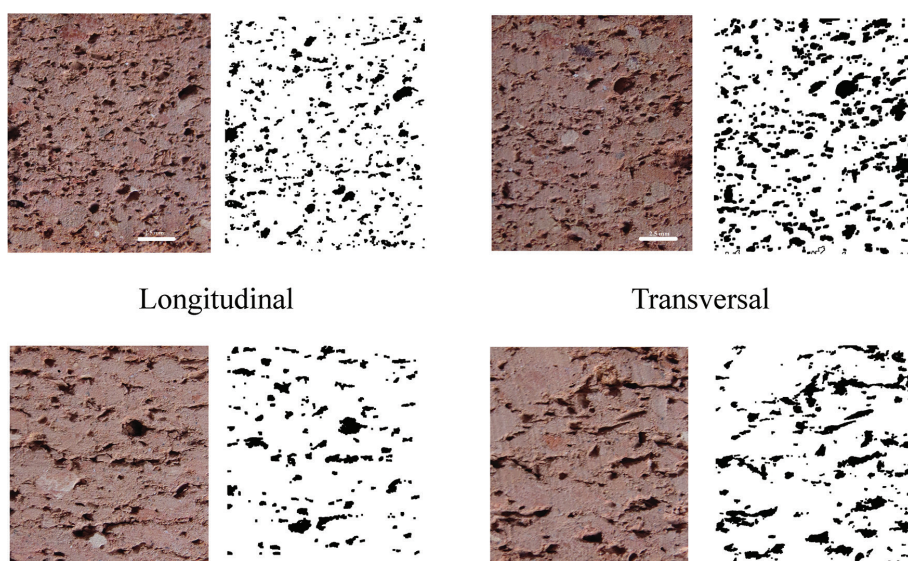


FIGURE 4. Examples of the variation of the porosity in transversal and longitudinal direction for sample M5 upper row and M2 lower row.

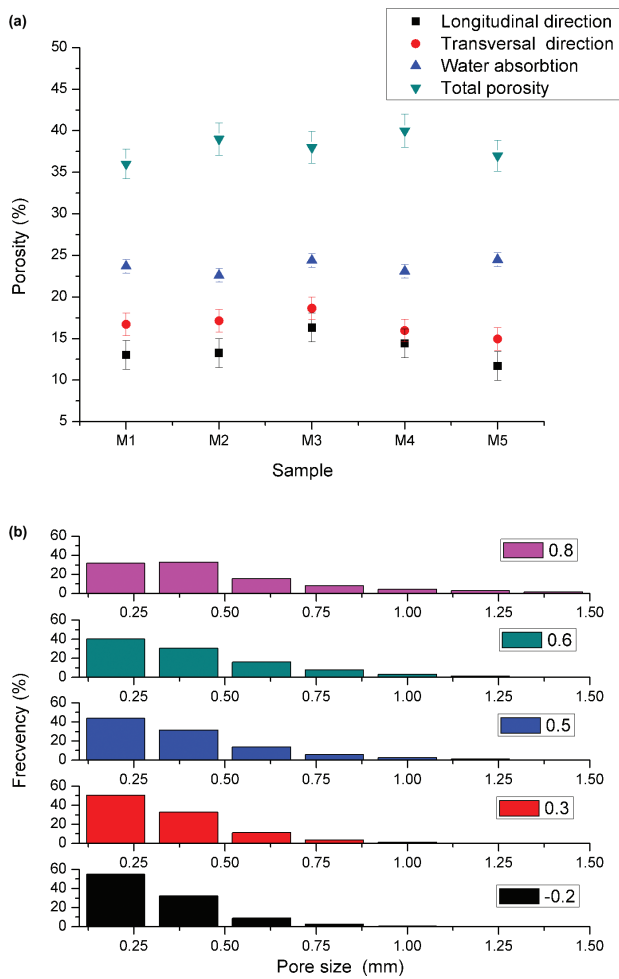


FIGURE 5. Porosity and pore size distribution obtained by image analysis on samples containing different fractions of sawdust particles.

The measured pore size fraction differs from the used sawdust particle at a first glance but is important to remember that the sawdust particles were separated by sieving, and during this process the particle passes through the mesh on its smallest section, and the image analysis in the used configuration measures all the pore's three dimensions. A gradual decrease of the pore size distribution is observed with the decrease of the used sawdust particles; in each case most of the pores have dimensions less than 0.5 mm. This can be explained by the elongated shape of the pores that varies from 0.3 up to 1 mm. Due to this variation the true dimensions of the pores vary from the calculated equivalent dimension.

Compressive strength on clay mixtures is between 7.9 MPa (M5) and 11.3 MPa (M1) (see Figure 6). One can observe a wide variation between samples for the same quantity of sawdust. Higher strengths occur in the case of samples M1, M2, which can be explained by the fact that the contact points between the clay particles are

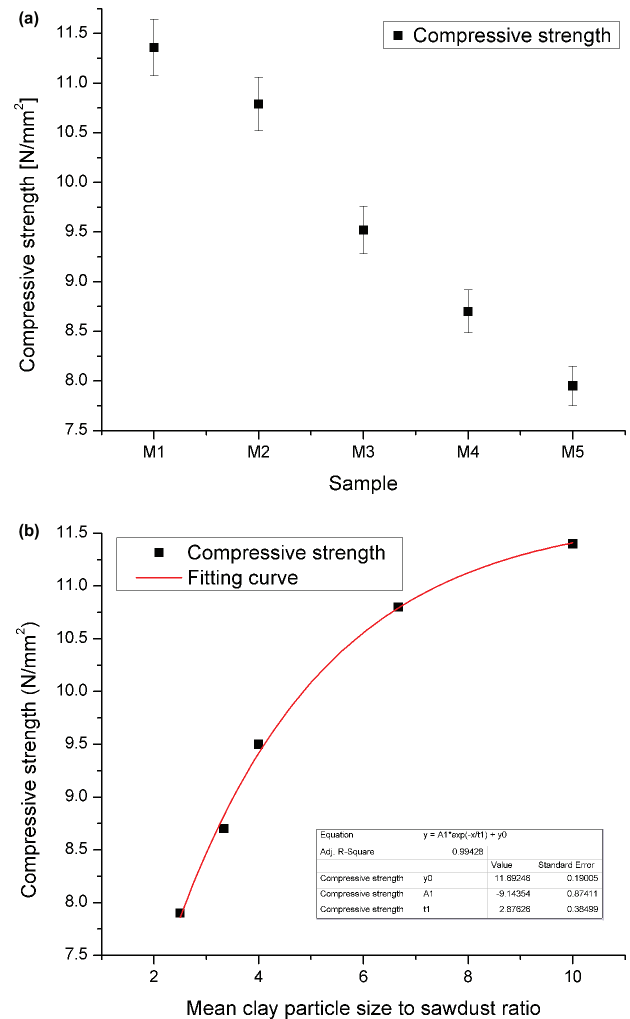


FIGURE 6. Compressive strength of the manufactured samples (a.) and its variation with the mean clay particle size to sawdust ratio (b.).

stronger and provide a better resistance to samples. As one can observe in Figure 4 a pore network is formed around the clay agglomerates, which tend to act as weak links between them even after firing. This fact explains the reduction of the mechanical properties. The effect of the coarser particles is due to the less bonding bridges between the clay agglomerates, the number of the bonding areas increases as the sawdust particle size decreases.

The thermal diffusivity of the pyroelectric sensor is independent on the thermal behaviour of the investigated sample. In this case, the sensor's thermal diffusivity is $\alpha = 1.1 \times 10^{-6} \text{ m}^2/\text{s}$, in good agreement with the literature. This result confirms the fact that the theoretical and the experimental conditions are fulfilled. The obtained results for the investigated samples (M1 - M5) are displayed in Figure 7. Figure 8 shows the optimization of the fits performed in order to get the thermal effusivity. The correct value of the thermal effusivity minimizes the

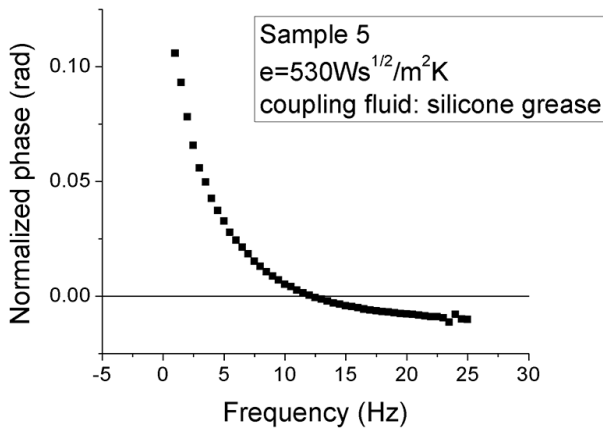


FIGURE 7. Normalized FPPE phase as a function of chopping frequency for M5.

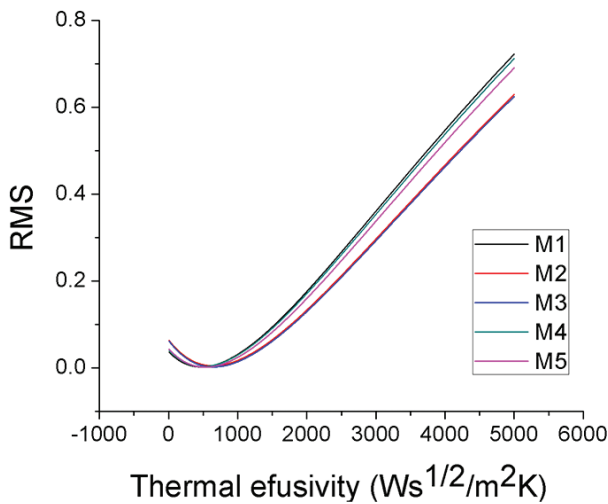


FIGURE 8. Root mean square deviation of the fit performed with Equation [1] on the experimental data (PPE phase as a function of chopping frequency), with sample's thermal effusivity as a fit parameter. The minimum of the curve indicates the value of the thermal effusivity.

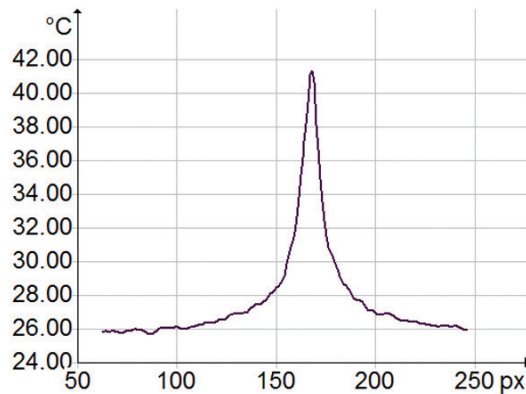
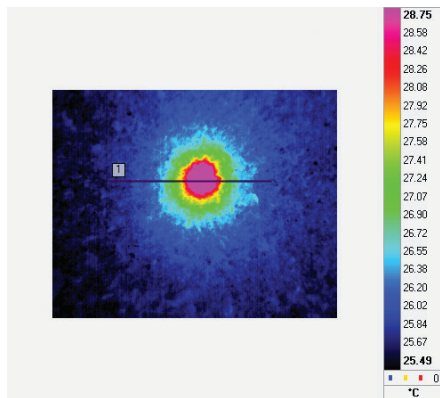


FIGURE 9. DC image (left) and the amplitude profile along the marked line (right) for M2.

root mean square (RMS) of the experimental data performed with Equation [1].

IR investigations: The DC amplitude and phase images, together with the corresponding profiles are shown in Figures 9-11. The DC and the amplitude images show the dissipation of the heat at the surface of the sample, due to the absorption of the laser. The profiles are quite smooth and thus the emissivity of the investigated surface can be assumed to be constant. The average temperature of the surface has increased from 26 °C up to 41 °C (see Figure 10). The profile of the phase image shows that the thermal wave diffuses to the surface of the sample symmetrically with respect to the excitation source (the laser is targeted close to the pixel 170 on the IR images). The thermal wave spreads over a distance of about 1.5 mm around the excitation source. The disturbance of the thermal wave (see the phase profile, around pixel 210) reveals the presence of a small pore located on the surface of the sample M2. The thermal diffusivity of the samples was calculated from phase profiles, according to Equation [4].

The obtained results with the associated standard deviations are listed in Table 2. The thermal effusivity was measured for all four transversal sections of a cubic specimen and the average value was calculated. The thermal diffusivity was taken on the same surface, at four different points, and the mean value was calculated.

The thermal conductivity values lie between 0.69W/mK (the control sample) and 0.49W/mK. The thermal conductivity of the samples containing pore-forming agent decreases by 30% compared to the reference sample. At the same time, the samples (M4 and M5) containing the sawdust particles with bigger size (0.6mm÷1.2mm) have a slightly lower conductivity (k=0.49 W/mK) compared to M2 and M3 samples (k=0.58W/mK) which contain the same percentage of pore-forming agent with smaller size (0.3mm÷0.6mm). May be observed that thermal conductivity coefficient

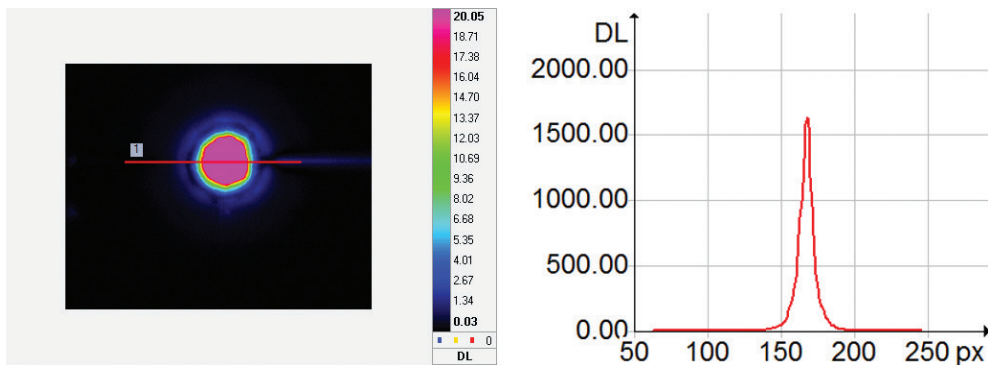


FIGURE 10. Amplitude image (left) and the amplitude profile along the marked line (right) for M2.

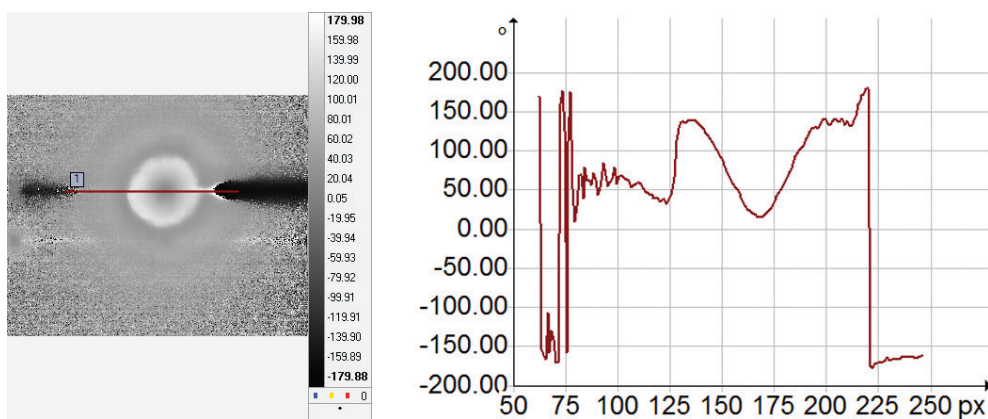


FIGURE 11. Phase image (left) and the amplitude profile along the marked line (right) for M2.

TABLE 2. Thermal conductivities of fired clay bricks in parallel and perpendicular directions.

Sample	k_{\perp}	k_{\parallel}	$(k_{\parallel})/(k_{\perp})$
M1	0.50 ± 0.05	0.58 ± 0.05	1.16
M2	0.57 ± 0.06	0.62 ± 0.04	1.08
M3	0.58 ± 0.06	0.63 ± 0.05	1.06
M4	0.49 ± 0.05	0.53 ± 0.04	1.08
M5	0.49 ± 0.04	0.54 ± 0.04	1.1
CS	0.69 ± 0.04	0.69 ± 0.06	1

is lower for samples with large particle size of sawdust which are in accordance with other authors observations (12, 23).

In the sections perpendicular to the pressing plane (transversal sections) the pore distribution is slightly larger than in the longitudinal direction (parallel with respect to the pressing plane), and the pores are quite elongated. Nevertheless, only a slight anisotropy in the thermal conductivity is revealed, as shown in Table 2. The heat flow is privileged in the parallel direction due to a slightly higher thermal conductivity. Compared to extruded bricks the ratio $k_{\parallel}/k_{\perp} \cong 1.1$ for conventional bricks is in the range

1.08-1.9 obtained by authors (7,11). Anisotropy of the sample appear due to the pore forming agent and clay layers orientation which affect the thermal and mechanical properties of pressed (10) and extruded clay bricks (7, 8, 11).

4. CONCLUSIONS

Room temperature X-ray diffraction shows that the starting crystalline phases are quartz, kaolinite, calcite, dolomite and some iron oxides. High temperature X-ray diffraction combined with the DTA-TGA-MS analysis shows that these phases are subjected to different transformations as follows: quartz suffers a transformation phase around 580°C , followed by the beginning of the dehydration of kaolinite. Around 720°C a sharp rise in the CO_2 partial pressure is observable in the MS curve correlated with a mass loss which corresponds to the calcite decomposition. Further increasing the temperature another peak in the CO_2 partial pressure is observable corresponding to the dolomite's decomposition. In the fired samples the different crystalline phases are present. The silicon dioxide reacts with the aluminum oxide (and forms mullite and illite), incorporating different other cations,

some quartz reacts with the iron and forms iron silicon dioxide. A significant quantity of iron oxide remains for the samples to have the specific reddish color.

The optical microscopy shows the formation of a high porosity pore network, significantly reducing the mechanical properties. A difference in the porosity determined by optical microscopy was observed along the length of the scaled down brick due to the anisotropic shape of the sawdust particles.

The pores size distribution measured by image analysis shows a decreasing trend with the decrease of the used sawdust particle size range. Water absorption and total porosity variation with particle size range is in the range of the experimental uncertainties, no clear trend is observable. Since the determining parameter is the porosity not the pore size distribution.

The effect of anisotropy in thermal transport is insignificant for conventional bricks, compared to ceramic block obtained by extrusion. The thermal conductivity is about 10% smaller in the perpendicular direction than in the longitudinal one. Thus, the laying directions of conventional bricks to the wall geometry is not critical such as the bricks obtained by extrusion.

On the other hand, the compressive strength follows a linear decrease due to the formation of the weak links between the clay particles. By increasing the sawdust particles size, the bigger pores act as more intense crack initiation sites, drastically reducing the samples compressive strength. Compared to the mean particle size of the starting mixture ($d_{50}=2.1$ mm) one can observe that the compressive strength increases with the increase of the clay particle/sawdust particle ratio.

ACKNOWLEDGMENTS

This work was supported by the Romanian National Authority for Scientific Research and Innovation, CNCS/CCCDI – UEFISCDI, project number PN-III-P2-2.1-BG-2016-0203, within PNCDI III, contract no. 71BG/2016.

References

1. Yükses, İ. (2015) The evaluation of building materials in terms of energy efficiency. *Period. Polytech-Civ.* 59 [1], 45–58. <https://doi.org/10.3311/PPci.7050>.
2. CR6-2013 (2013) Design code for masonry structures. Romania: Monitorul Oficial.
3. P100-1/2013 (2014) Seismic design code—Part I—Design provisions for buildings. Romania: Monitorul Oficial.
4. SR EN 1996-2:2006 (2006) Eurocode 6. Design of masonry structures—part 2: design considerations, selection of materials and execution of masonry. Romania: ASRO.
5. Hassan, A.M.; Moselhy, H.; Abadir, M.F. (2019) The use of bagasse in the preparation of fireclay insulating bricks. *Int. J. Appl. Ceram. Tec.* 16 [1], 418–425. <https://doi.org/10.1111/ijac.13094>.
6. Cobirzan, N.; Thalmaier, Gy.; Balog, A.A.; Constantinescu, H.; Timis, I.; Streza, M. (2018) Thermophysical properties of fired clay bricks with waste ceramics and paper pulp as pore-forming agent. *J. Therm Anal Calorim.* 134 [1], 843–851. <https://doi.org/10.1007/s10973-018-7092-3>.
7. Maillard, P.; Aubert, J.E. (2014) Effects of anisotropy of extruded earth bricks on their hygrothermal properties. *Constr. Build. Mater.* 63, 56–61. <https://doi.org/10.1016/j.conbuildmat.2014.04.001>.
8. Aubert, J.E.; Maillard, P.; Morel, J.C.; Al Rafii M. (2016) Towards a simple compressive strength test for earth bricks? *Mater. Struct.* 49 [5], 1641–1654. <https://doi.org/10.1617/s11527-015-0601-y>.
9. Korah, L.V.; Nigay, P.M.; Cutard, T.; Nzihou, A.; Thomas, S. (2016) The impact of the particle shape of organic additives on the anisotropy of a clay ceramic and its thermal and mechanical properties. *Constr. Build. Mater.* 125, 654–660. <https://doi.org/10.1016/j.conbuildmat.2016.08.094>.
10. Balog, A.A.; Cobirzan, N.; Thalmaier, Gy.; Constantinescu, H.; Voinea, M. (2019) Psyllium Seeds Used as Pore Forming Agent in Clay Bricks. *Procedia Manuf.* 32, 242–247. <https://doi.org/10.1016/j.promfg.2019.02.209>
11. Aouba, L.; Coutand, M.; Perrin, B.; Lemercier, H. (2015) Predicting thermal performance of fired clay bricks lightened by adding organic matter: Improvement of brick geometry. *J. Build. Phys.*, 38 [6], 531–547. <http://dx.doi.org/10.1177/1744259115571078>.
12. Bwayo, E.; Obwoya, S.K. (2014) Coefficient of Thermal Diffusivity of Insulation Brick Developed from Sawdust and Clays. *J. Ceram.* 2014, 1–6. <https://doi.org/10.1155/2014/861726>.
13. Demir, I. (2008) Effect of organic residual addition on the technological properties of clay bricks. *Waste Manage.* 28 [3], 622–627. <https://doi.org/10.1016/j.wasman.2007.03.019>.
14. Kadir, A.A.; Sarani, N.A. (2012) An overview of waste recycling in fired clay bricks. *Int. J. of Integrated Engineer.* 4 [2], 53–69.
15. Chemani, B.; Chemani, H. (2012) Effect of adding sawdust on mechanical-physical properties of ceramic bricks to obtain lightweight building material. *Int. J. Mech. Aerosp. Industrial Mechatron. Manuf. Eng.* 6 [11], 2521–2525. <https://doi.org/10.5281/zenodo.1077395>.
16. Sutcu, M.; Akkurt, S. (2009) The use of recycled paper processing residues in making porous brick with reduced thermal conductivity. *Ceram. Intern.* 35 [7], 2625–2631. <https://doi.org/10.1016/j.ceramint.2009.02.027>.
17. Bories, C.; Aouba, L.; Vedrenne, E.; Vilarem, G. (2015) Fired clay bricks using agricultural biomass wastes: Study and Characterization. *Constr. Build. Mater.* 91, 158–163. <https://doi.org/10.1016/j.conbuildmat.2015.05.006>.
18. Barbieri, L.; Andreola, F.; Lancellotti, I.; Taurino, R. (2013) Management of agricultural biomass wastes: preliminary study on characterization and valorization in clay matrix bricks. *Waste Manag.* 33 [11], 2307–2315. <https://doi.org/10.1016/j.wasman.2013.03.014>.
19. Georgiev, A.; Yoleva, A.; Djambazov, S.; Dimitrov, D.; Ivanova, V. (2018) Effect of expanded vermiculite and expanded perlite as pore forming additives on the physical properties and thermal conductivity of porous clay bricks. *J. Chem. Technol. Metall.* 53 [2], 275–280. https://dl.uctm.edu/journal/node/j2018-2/14_17_76_p_275_280.pdf.
20. Demirbaş, A. (1997) Calculation of higher heating values of biomass fuels. *Fuel*, 76 [5], 431–434. [https://doi.org/10.1016/S0016-2361\(97\)85520-2](https://doi.org/10.1016/S0016-2361(97)85520-2).
21. Okunade, E.A. (2008) The effect of wood ash and sawdust admixtures on the engineering properties of a burnt laterite-clay brick. *J. Appl. Sci.* 8 [6] 1042–1048. <https://doi.org/10.3923/jas.2008.1042.1048>.
22. Chemani, H.; Chemani, B. (2013) Valorization of wood sawdust in making porous clay brick. *Sci. Res. Essays* 8 [15] 609–614. <https://academicjournals.org/journal/SRE/article-abstract/58926ED32710>.
23. Bwayo, E.; Obwoya, S.K. (2014) Thermal Conductivity of insulation brick developed from sawdust and selected Uganda clays. *Int. J. Res. Eng. Technol.* 03 [09] 282–285. <https://doi.org/10.15623/ijret.2014.0309043>.

24. Ducman, V.; Kopar, T (2007) The influence of different waste additions to clay-product mixtures. *Materiali in tehnologije / Mater. Technol.* 41 [6] 289–293.
25. SR EN 772-21:2011 Methods of test for masonry units - Part 21: Determination of water absorption of clay and calcium silicate masonry
26. SR EN 772-13:2001 Methods of test for masonry units - Part 13: Determination of net and gross dry density of masonry units (except for natural stone)
27. Cobirzan, N.; Balog A.-A.; Belan, B.; Borodi, G.; Dadarlat, D.; Streza, M. (2016) Thermophysical properties of masonry units: Accurate characterization by means of photothermal techniques and relationship to porosity and mineral composition. *Constr. Build. Mater.* 105, 297–306. <https://doi.org/10.1016/j.conbuildmat.2015.12.056>.
28. García-Ten, J.; Orts, M.J.; Saburit, A.; Silva, G. (2010) Thermal conductivity of traditional ceramics: Part II: Influence of mineralogical composition. *Ceram. Int.* 36 [7], 2017–2024. <https://doi.org/10.1016/j.ceramint.2010.05.013>.
29. Dabare, L.; Svinka, R. (2013) Influence of thermal treatment and combustible additives on properties of Latvian clay ceramics pellets. *Process. Appl. Ceram.* 7 [4], 175–180. <https://doi.org/10.2298/PAC1304175D>.